Cellular/Molecular

Novel *SCN9A* Mutations Underlying Extreme Pain Phenotypes: Unexpected Electrophysiological and Clinical Phenotype Correlations

Edward C. Emery,[1]* Abdella M. Habib,[2]* James J. Cox,[2]* Adeline K. Nicholas,[3] Fiona M. Gribble,[1] C. Geoffrey Woods,[3] and Frank Reimann[1]

[1]University of Cambridge, Wellcome Trust/MRC Institute for Metabolic Science, Addenbrooke's Hospital, Cambridge, CB2 0QQ, United Kingdom, [2]University College London, Molecular Nociception Group, London, WC1E 6BT, United Kingdom, and [3]University of Cambridge, Cambridge Institute for Medical Research, Addenbrooke's Hospital, Cambridge, CB2 0XY, United Kingdom

The importance of $Na_V1.7$ (encoded by *SCN9A*) in the regulation of pain sensing is exemplified by the heterogeneity of clinical phenotypes associated with its mutation. Gain-of-function mutations are typically pain-causing and have been associated with inherited erythromelalgia (IEM) and paroxysmal extreme pain disorder (PEPD). IEM is usually caused by enhanced $Na_V1.7$ channel activation, whereas mutations that alter steady-state fast inactivation often lead to PEPD. In contrast, nonfunctional mutations in *SCN9A* are known to underlie congenital insensitivity to pain (CIP). Although well documented, the correlation between *SCN9A* genotypes and clinical phenotypes is still unclear. Here we report three families with novel *SCN9A* mutations. In a multiaffected dominant family with IEM, we found the heterozygous change L245 V. Electrophysiological characterization showed that this mutation did not affect channel activation but instead resulted in incomplete fast inactivation and a small hyperpolarizing shift in steady-state slow inactivation, characteristics more commonly associated with PEPD. In two compound heterozygous CIP patients, we found mutations that still retained functionality of the channels, with two C-terminal mutations (W1775R and L1831X) exhibiting a depolarizing shift in channel activation. Two mutations (A1236E and L1831X) resulted in a hyperpolarizing shift in steady-state fast inactivation. To our knowledge, these are the first descriptions of mutations with some retained channel function causing CIP. This study emphasizes the complex genotype–phenotype correlations that exist for *SCN9A* and highlights the C-terminal cytoplasmic region of $Na_V1.7$ as a critical region for channel function, potentially facilitating analgesic drug development studies.

Key words: **congenital insensitivity to pain; inherited erythromelalgia; Nav1.7; pain; paroxysmal extreme pain disorder; SCN9A**

Introduction

Naturally occurring mutations in *SCN9A* have been linked with both hyposensitive and hypersensitive pain states, emphasizing the important role of the encoded ion channel $Na_V1.7$ in the regulation of nociceptive neuron excitability (Dib-Hajj et al., 2013). Gain-of-function mutations in *SCN9A* are linked with debilitating, chronic pain syndromes, typified by inherited erythromelalgia (IEM), paroxysmal extreme pain disorder (PEPD), and small-fiber neuropathy (SFN). IEM and PEPD are rare but clinically distinct conditions; IEM is characterized by an episodic burning sensation in the hands and feet that is often coupled with redness and swelling, whereas PEPD is associated with extreme bouts of pain within proximal regions of the body, typically rectal and ocular. Patients with idiopathic SFN present with more widespread axonal degeneration resulting in pain and other sensory impairments, and a recent report found *SCN9A* mutations in 8 of 28 affected individuals (Faber et al., 2012). Loss-of-function mutations, by contrast, have been associated with a complete absence of pain in affected individuals, a condition known as congenital insensitivity to pain (CIP).

Electrophysiological characterization has revealed that, like other voltage-gated sodium channels, $Na_v1.7$ shows voltage-dependent activation and inactivation, with the latter having fast and slow components. Known *SCN9A*-associated CIP mutations are incapable of supporting functional $Na_V1.7$ expression, suggesting a crucial role of this current for nociception (Cox et al.,

Received Sept. 23, 2014; revised Feb. 25, 2015; accepted March 23, 2015.

Author contributions: E.C.E., J.J.C., F.M.G., C.G.W., and F.R. designed research; E.C.E., A.M.H., J.J.C., and A.K.N. performed research; E.C.E., A.M.H., J.J.C., A.K.N., C.G.W., and F.R. analyzed data; E.C.E., J.J.C., F.M.G., C.G.W., and F.R. wrote the paper.

J.J.C. and A.M.H. were supported by an MRC Research Career Development fellowship. F.M.G., F.R., and E.C.E. were supported by Wellcome Trust Senior Fellowships WT088357/Z/09/Z and WT084210/Z/07/Z and MRC Grant MC_UU_12012/3. C.G.W. was supported by the Cambridge Biomedical Research Campus. We thank Dr. Tony Jackson for helpful discussions while preparing this manuscript.

The authors declare no competing financial interests.

*E.C.E., A.M.H., and J.J.C. contributed equally to this work.

This article is freely available online through the *J Neurosci* Author Open Choice option.

Correspondence should be addressed to either Dr. Frank Reimann, University of Cambridge, Institute of Metabolic Science, Addenbrooke's Hospital, Hills Road, Cambridge CB2 0QQ, United Kingdom. E-mail: fr222@cam.ac.uk. or Prof. C. Geoffrey Woods, University of Cambridge, Cambridge Institute for Medical Research, Addenbrooke's Hospital, Hills Road, Cambridge CB2 0XY, United Kingdom. E-mail: cw347@cam.ac.uk.

DOI:10.1523/JNEUROSCI.3935-14.2015

2006, 2010) and the essential dependence of nociception on Nav1.7 was recently confirmed in mice (Gingras et al., 2014). SFN mutations appear to impair the slow inactivation of Nav1.7 currents, and it has been suggested that the resulting overexcitability results in an increased sensitivity of small-diameter DRG neurons to otherwise benign insults (Faber et al., 2012). Overexcitability is also observed when mutations found in patients with IEM or PEPD are heterologously expressed in DRG neurons (Dib-Hajj et al., 2008; Estacion et al., 2008; Eberhardt et al., 2014); however, the underlying electrophysiological characteristics of the mutated $Na_V1.7$ are thought to differ from each other. IEM mutations generally cause a hyperpolarizing shift in channel activation, whereas PEPD is typically associated with a depolarizing shift in fast inactivation (albeit often incomplete), resulting in persistent and/or resurgent currents. Why, or how, subtle changes in channel gating result in different phenotypes is currently unclear, but rare mutations found in patients with mixed IEM and PEPD symptoms have been shown to simultaneously display altered activation and inactivation properties (Estacion et al., 2008).

To further understand the effects of discrete molecular and functional changes in both hyposensitive and hypersensitive pain conditions, we electrophysiologically characterized four novel mutations in $Na_V1.7$ identified in two individual cases of CIP (W1775R, A1236E, L1831X) and one case of IEM (L245V). Surprisingly, all three CIP-related mutations gave rise to functional $Na_V1.7$ channels, exhibiting changes in activation and/or fast inactivation gating properties, coupled with a significant reduction in total current. In contrast, the single IEM-related mutation showed no change in channel activation properties but did show significant changes in inactivation properties. Our results challenge a simple correlation between electrophysiological properties observed *in vitro* and patient phenotype.

Materials and Methods

Identification of novel SCN9A mutations. The cases reported here were sequentially ascertained from a British National Health Service molecular genetics laboratory service offering Mendelian pain gene sequencing. Cases of either sex referred to our service have both excess or lack of pain phenotypes, and *SCN9A* is one of the human genes we routinely screen. Genomic DNA was isolated from peripheral blood by standard methods. All coding exons and flanking splice sites of *SCN9A* were bidirectionally sequenced using previously reported primers (Cox et al., 2006).

Construction of expression plasmids. The wild-type *SCN9A*-polio IRES-*DsRed2* construct (FLRED) and the *SCN1B*-encephalomyocarditis virus-*SCN2B*-polio IRES-*EGFP* (JC5) construct were generated as previously described (Cox et al., 2006). These bear either *SCN9A* and *DsRed2* (FLRED) or *SCN1B*, *SCN2B*, and *EGFP* (JC5) on the same vector expressed from the same promoter, and the inclusion of *DsRed2* and *EGFP* in these constructs helped in the identification of positively cotransfected cells when patch clamping. The $Na_v1.7$-L245V, $Na_v1.7$-A1236E, $Na_v1.7$-A1632E, $Na_v1.7$-W1775R, and $Na_v1.7$-L1831X mutations were introduced into FLRED using the QuikChange II XL Site-Directed Mutagenesis Kit (Stratagene) or by recombinant PCR.

Cell culture and transfection. HEK293 cells were used for all experiments. Briefly, HEK293 cells were maintained in a 75 cm^2 flask with DMEM (4500 mg/L glucose) supplemented with 5% FBS, L-glutamine, and penicillin/streptomycin (culture medium) at 37°C, 5% CO_2. Cells were split every third day of culture. For transfection, HEK293 cells were plated directly onto 35 mm plastic dishes (Falcon) and incubated for 24 h at 37°C, 5% CO_2. After 24 h, the culture medium was replaced and the cells were incubated for 30 min. After 30 min, 500 μl of Optimem (Invitrogen) containing 1 μg of *SCN9A* cDNA (mutant or wild-type), 42.5 ng of β_1/β_2 cDNA, and 10 μl of lipofectamine 2000 (Invitrogen) was added to each dish of cells, which were then incubated for 24 h at 37°C, 5% CO_2. For the negative control, β_1/β_2 cDNA (42.5 ng) was transfected alone. After 24 h, the cells were split and diluted 1:20 in culture medium and plated directly onto 35 mm dishes and incubated for 24 h. All cells were recorded from 24 to 48 h after transfection.

Electrophysiological analysis. All electrophysiological recordings were performed using an AxoPatch 200B amplifier and a Digidata 1440A digitizer (Axon Instruments), controlled by Clampex software (version 10, Molecular Devices). Filamented borosilicate microelectrodes (GC150TF-15, Harvard Apparatus) were coated with beeswax and fire polished using a microforge (Narishige) to give resistances of 2–3 MΩ. For voltage-clamp experiments, the following solutions were used. Extracellular solution (values are in mM) as follows: 140 NaCl, 3 KCl, 1 $MgCl_2$, 2 $CaCl_2$, 10 HEPES, 1 glucose, pH 7.4 with NaOH. Intracellular solution (values in mM) as follows: 107 CsF, 10 EGTA, 10 TEA.Cl, 2 $MgCl_2$, 10 HEPES, 10 NaCl, 1 $CaCl_2$, pH 7.2 with CsOH. Unless otherwise stated, standard whole-cell currents were acquired at 25 kHz and filtered at 10 kHz (low-pass Bessel filter) at 22°-24°C. After achieving whole-cell configuration, a holding potential of −100 mV was applied and series resistance was compensated by 70%. All currents were leak subtracted using a p/4 protocol. Liquid junction potentials were calculated using Clampex software and corrected for before analysis. For resurgent current recordings, the β4 peptide (KKLITFILKKTREK, Invitrogen) was included in the intracellular pipette solution at 100 μM. The peptide was added on the day of experiment from a 10 mM stock (ddH_2O). Voltage-dependent activation was fitted to a Boltzmann equation $y = (A2 + (A1 - A2)/(1 + exp((V_h - x)/k))) * (x - V_{rev})$, where $A1$ is the maximal amplitude, V_h is the potential of half-maximal activation, x is the clamped membrane potential, V_{rev} is the reversal potential, and k is a constant. Voltage dependence of inactivation was fitted to a single Boltzmann equation: $y = (A1 - A2)/(1 + exp((x - V_h/k)) + A2$, or a double Boltzmann equation: $y = y0 + A * (frac/(1 + exp((x - x01)/k1)) + (1 - frac)/(1 + exp((x - x02)/k2)))$, where $k1$ and $k2$ were constrained to 4.5. All Boltzmann equations were fitted using Origin software. Voltage dependence of channel deactivation was fitted to a double exponential of the form: $f(t) = Af\ exp\ (-t/\tau_f) + As\ exp\ (-t/\tau_s) + C$, using Clampfit software.

Data analysis. All electrophysiological data were extracted using Clampfit (version 10, Molecular Devices) and analyzed using Origin 9.0 (OriginLab). Significance was determined at $p < 0.05$. Individual p values are given for each comparison made.

Results

Identification of novel SCN9A mutations and patient phenotype

A large family with an inherited erythromelalgia phenotype and two unrelated individuals with apparent congenital insensitivity to pain were referred to us for genetic testing (for location of novel mutations in $Na_V1.7$, see Fig. 1).

Family 1. The index case referred to us suffered from severe episodic pain in his hands and feet associated with excess heat perception. Three other members of the family were similarly affected and another five cases suspected according to family history. The painful episodes usually became distressing in the second decade of life but retrospectively started approximately a decade earlier. Episodes were precipitated by exercise, hot weather, and viral illness, and soothed by cold. Attacks usually started with pain restricted to the surface of the affected body part, but later during an episode pain was also perceived deeper within the tissue; during an attack, the affected part of the body exhibited allodynia and erythema, but this was not usually accompanied by swelling. The episodes tended to get more frequent and of greater severity with age; however, family members have developed a number of strategies to minimize the number and severity of the attacks, such as exercising in bare feet and wearing open sandals. Attacks could reliably be aborted by cooling within the first 5 min, but not thereafter. The pain phenotype was inherited as a dominant trait,

with both males and females similarly affected and passage from mother to son and father to daughter. Other possible causes of erythromelalgia had previously been excluded; and importantly, none of the affected family members reported pain on defecating or in facial (ocular) areas. We found the novel heterozygous *SCN9A* change c.733C>G (causing the $Na_V1.7$ change p.L245V) in the referred index case. We thence confirmed that three other clinically affected individuals bore the mutation, whereas one clinically unaffected individual who requested testing did not.

Family 2. The index case was a 5-year-old girl referred to us as having no evidence of feeling pain. She had not shown any signs of distress during early life's immunizations or teething but lacked any injuries to her lips, tongue, or terminal digits often seen in other individuals with congenitally inherited insensitivity to pain. However, the parents became concerned that she failed to respond appropriately to repeated falls and minor injuries, culminating with her developing a limp when 3 years of age and being found to have a fractured femur. She complained of no pain during this episode, and once placed in a plaster cast the bone healed normally. As speech developed, she was able to articulate that she did not feel discomfort or pain after injuries or falls but realized that other people found these events unpleasant. Her development and general health were normal. We tested the patient by applying pressure with a rigid 0.8 cm plastic tube onto the proximal region of the nail bed of the index finger while the patient's hand lay flat on a hard unyielding surface. This procedure does not result in lasting damage to the nail or bruising, but control individuals report touch sensation at gentle pressures applied, which disappears immediately upon removal of the weight and pain lasting ~10 s when the applied weight exceeds ~1 kg. The patient, by contrast, could perceive pressure but did not report any unpleasant sensation at maximal applied weights exceeding ~10 kg. The patient was also anosmic. Screening of *SCN9A* identified two mutations, which were inherited from her parents, who each also carried a wild-type allele and had normal pain perception. The mutations identified are a mutation in the canonical splice donor site of exon 7 from GTATG to GTATC c.901 + 5G>C expected to give rise to misplicing, which would be expected to trigger nonsense mediated decay and a missense *SCN9A* mutation c.5323T>A (causing the $Na_V1.7$ change p.W1775R).

Family 3. The index case was a 12-year-old boy, who had been adopted at age 6 and his prior early history was unknown. He had always appeared to have a high pain tolerance responding little to injuries and accidents, while being intolerant of others distress. He had accumulated a number of scars from injuries on his limbs, had burn scars on his hand, and a chronic long-standing injured ankle that had never properly healed (a Charcot's joint). His intelligence and general health appeared normal. He is anosmic and did not report to feel any pain when pressure was applied to the nail bed of his index finger (see above). Screening of SCN9A identified two mutations, a missense mutation c.3707C>A (causing the $Na_V1.7$ change p.A1236E) and the nonsense mutation c.5492T>G (causing the $Na_V1.7$ change p. L1831X). This latter nonsense mutation occurred in the terminal exon of SCN9A and would be expected to lead to a stable mRNA product and a prematurely truncated protein missing the C-terminal 146 amino acids of the protein. Subsequent screening of the birth parents genotype was not possible.

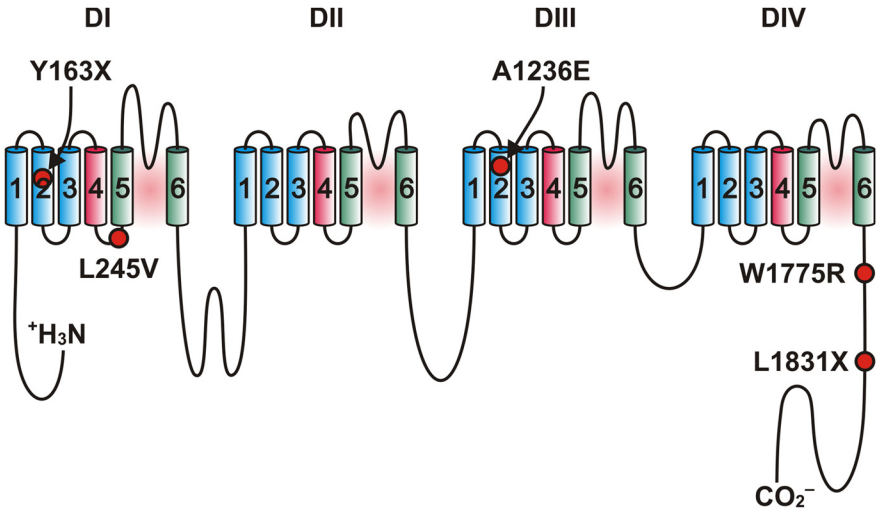

Figure 1. Location of characterized CIP and IEM-associated mutations in $Na_V1.7$. Schematic representation of $Na_V1.7$ showing the 24 trans-membrane (TM) domains contained within four regions (DI-IV). Within each region, there are six TM domains. The fourth TM domain within each region acts as the voltage sensor (red), whereas TM domains 5 and 6 come together to form the channel pore (green). The proposed location for each mutation is shown. Y163X (CIP) is located within the second TM domain of the first region (not studied). L245V (IEM) is located within the intracellular loop between domains 4 and 5 of the first region. A1236E (CIP) is located within the second TM domain of the third region. W1775R (CIP) and L1831X (CIP) are both located within the intracellular C-terminal tail.

Characterization of novel CIP-associated mutations

To further understand the link between molecular and functional changes in $Na_V1.7$ channels in the CIP cases, electrophysiological analysis was performed on three of the mutations identified in Families 2 and 3: W1775R, A1236E, and L1831X. Individual parameter comparisons are summarized in Table 1. Rather intriguingly, all three mutants gave rise to functional channels, giving averaged peak activation currents of −115.9 ± 15.0, − 41.0 ± 11.9, and −103.3 ± 14.0 pA/pF for W1775R, A1236E, and L1831X, respectively (Fig. 2*A–F*). The peak activation currents from mutant channels were significantly smaller than the peak current for WT $Na_V1.7$ (−361 ± 39.5 pA/pF); however, they were substantially bigger than the β_1/β_2 negative control (8.9 ± 1.1 pA/pF). With respect to gating properties, the V_h of channel activation for W1775R and L1831X was shifted significantly to more depolarized potentials (−13.4 ± 1.3 and −15.4 ± 1.8 mV, respectively) compared with WT (−25.2 ± 1.6 mV), whereas A1236E exhibited no significant shift (−21.5 ± 1.8 mV). In addition, the steepness of the voltage dependence, *k*, was significantly shallower for W1775R (−7.5 ± 0.2), A1236E (−7.3 ± 0.4), and L1831X (−7.6 ± 0.2) compared with WT (−3.7 ± 0.3). No change in reversal potential (V_{rev}) was observed between WT, mutant, or β_1/β_2 negative control currents, consistent with Na^+-selective currents. Analysis of fast inactivation properties showed that A1236E and L1831X exhibited a hyperpolarizing shift in V_h values (−80.7 ± 1.3 and −82.2 ± 1.3 mV, respectively) compared with WT (−71.1 ± 1.3 mV), whereas no significant difference was observed with W1775R (−73.4 ± 2.2 mV) (Fig. 2*B*,*D*,*F*). In addition, there was a significant difference in the slope *k* of channel inactivation for W1775R (11.6 ± 1.1),

Table 1. Summary of channel gating parameters for WT and mutant $Na_V1.7$ channels[a]

	WT	W1775R	A1236E	L1831X	L245V	β_1/β_2 only
Activation						
$V_{0.5}$ (mV)	−25.2 ± 1.6	−13.4 ± 1.3, $p = 5.24E-4$	−21.5 ± 1.8	−15.4 ± 1.8, $p = 1.50E-3$	−25.2 ± 1.3	−30.3 ± 4.9
k	−3.7 ± 0.3	−7.5 ± 0.2, $p = 1.54E-6$	−7.3 ± 0.4, $p = 3.54E-6$	−7.6 ± 0.2, $p = 1.30E-7$	−4.9 ± 0.4, $p = 2.16E-2$	−9.5 ± 1.2, $p = 6.72E-7$
V_{Rev} (mV)	67.5 ± 2.3	71.4 ± 4.9	67.5 ± 3.8	72.5 ± 5.3	74.0 ± 3.1	76.9 ± 15.5
I_{max} (pA.pF^{-1})	−361.2 ± 39.5	−115.9 ± 15.0, $p = 2.24E-3$	−41.0 ± 11.9, $p = 5.75E-5$	−103.3 ± 14.0, $p = 3.73E-4$	−398.5 ± 44.7	−8.9 ± 1.1, $p = 1.18E-4$
n	23	7	8	9	16	6
Fast inactivation						
$V_{0.5}$ (mV)	−71.1 ± 1.3	−73.4 ± 2.2	−80.7 ± 1.3, $p = 3.22E-4$	−82.2 ± 1.3, $p = 2.82E-5$	—	−72.6 ± 4.4
k	6.1 ± 0.4	11.6 ± 1.1, $p = 1.68E-5$	9.1 ± 0.8, $p = 1.91E-3$	7.9 ± 0.6, $p = 2.38E-2$	—	8.2 ± 1.7
n	22	7	8	9		6
DB fast inactivation						
$V_{0.5}$ (mV) #1	—	—	—	—	71.2 ± 0.6	—
$V_{0.5}$ (mV) #2	—	—	—	—	31.4 ± 1.8	—
n					10	
Slow inactivation						
$V_{0.5}$ (mV)	−31.4 ± 1.8	—	—	—	−41.4 ± 0.9, $p = 4.00E-4$	
k	9.9 ± 0.6	—	—	—	11.3 ± 1.7	—
n	8				16	

[a]The table shows averaged parameters for channel activation, fast inactivation, and slow inactivation for WT and mutant $Na_V1.7$ channels (W1775R, A1236E, L1831X, and L245V), as well as the β_1/β_2 subunit. Fast inactivation values for L245V are under a separate entry because of the double Boltzmann fit (DB fast inactivation). Data are mean ± SEM. All values are compared with the averaged WT value. p value is given for comparisons that are deemed significantly different ($p < 0.05$). All single-parameter comparisons were tested using an unpaired two-way Student's t test.

A1236E (9.1 ± 0.8), and L1831X (7.9 ± 0.6), compared with WT (6.1 ± 0.4).

Characterization of a novel IEM-associated mutation

Electrophysiological analysis was performed on the IEM-associated $Na_V1.7$ mutation, L245V. Individual parameter comparisons are summarized in Table 1. Analysis of channel activation properties showed that L245V gave rise to functional channels and exhibited peak activation currents that were not significantly different to WT (−398.5 ± 44.7 and −361.2 ± 39.5 pA/pF, respectively; Fig. 3*A*). Furthermore, L245V and WT activation currents exhibited almost identical V_h values (−25.2 ± 1.3 and −25.2 ± 1.6 mV, respectively), with V_{rev} values also being comparable. There was, however, a modest, but significant, change in the slope (k) for L245V (−4.9 ± 0.4) compared with WT (−3.7 ± 0.3). Fast inactivation properties were also investigated for L245V. In contrast to WT, L245V fast inactivating currents were fitted with a double Boltzmann, with the first V_h value ($V_{h\#1}$; −71.2 ± 0.6 mV) of the double Boltzmann fit being similar to V_h for WT currents (−71.1 ± 1.3 mV) (Fig. 3*B*). Interestingly, L245V currents exhibited incomplete fast inactivation, leaving a substantial persistent current remaining even 500 ms following initial channel activation at several test pulses (Fig. 3*B*,*D*), and it is likely that the inability of L245V channels to fully undergo fast inactivation allows a secondary slower inactivation process with rightward shifted voltage dependence to become apparent. In addition to incomplete fast inactivation, L245V also exhibited a significant hyperpolarizing shift in the V_h of slow inactivation (L245V: −41.4 ± 0.9 mV; WT: −31.4 ± 1.8 mV), a slowing of deactivation kinetics (L245V: 0.20 ± 0.02 ms; WT: 0.09 ± 0.1 ms at −60 mV), as well as an increased ramp current in response to a depolarizing ramp stimulus (Fig. 3*E*–*G*). We next investigated whether the changes in channel inactivation associated with L245V give rise to the emergence of resurgent currents by including the β4 peptide (KKLITFILKKTREK; 100 μM) in the intracellular pipette solution. We were, however, unable to detect clear resurgent currents beyond the observed tail currents in the absence of the β-4 peptide for the wild-type, the L245V mutation, or the previously described A1632E mutation (Fig 3*C*).

Discussion

Given the fundamental role of $Na_V1.7$ ion channels in pain, understanding how molecular and functional changes affect sensory nerve function could facilitate the development of novel analgesics, as well as improve current treatment strategies for related chronic pain syndromes. In this study, we identified and electrophysiologically characterized four naturally occurring novel mutations in $Na_V1.7$ that give rise to either hyposensitive (CIP) or hypersensitive (IEM) pain conditions.

The link between $Na_V1.7$ functional change and pathogenesis

Previous studies have concluded that pain-insensitive mutations are due to a total loss of $Na_V1.7$ channel function (Cox et al., 2006, 2010; Ahmad et al., 2007), which, given the fundamental role of $Na_V1.7$ in regulating electrical activity in sensory neurons, intuitively explains the painless phenotype. Here, however, we present three novel CIP-associated mutations in $Na_V1.7$ that all retain some functionality. Electrophysiological characterization of the three mutations showed that each had a significant reduction in peak current following activation, compared with WT. In addition, each mutation also exhibited changes in activation and/or inactivation properties. Both W1775R and L1831X exhibited an ~10 mV depolarizing shift in channel activation, whereas A1236E and L1831X exhibited a similar hyperpolarizing shift in channel fast inactivation. Such changes in channel activation/inactivation properties would have the effect of reducing the number of channels activated, as well as reducing the number of channels available for activation, respectively, which would ulti-

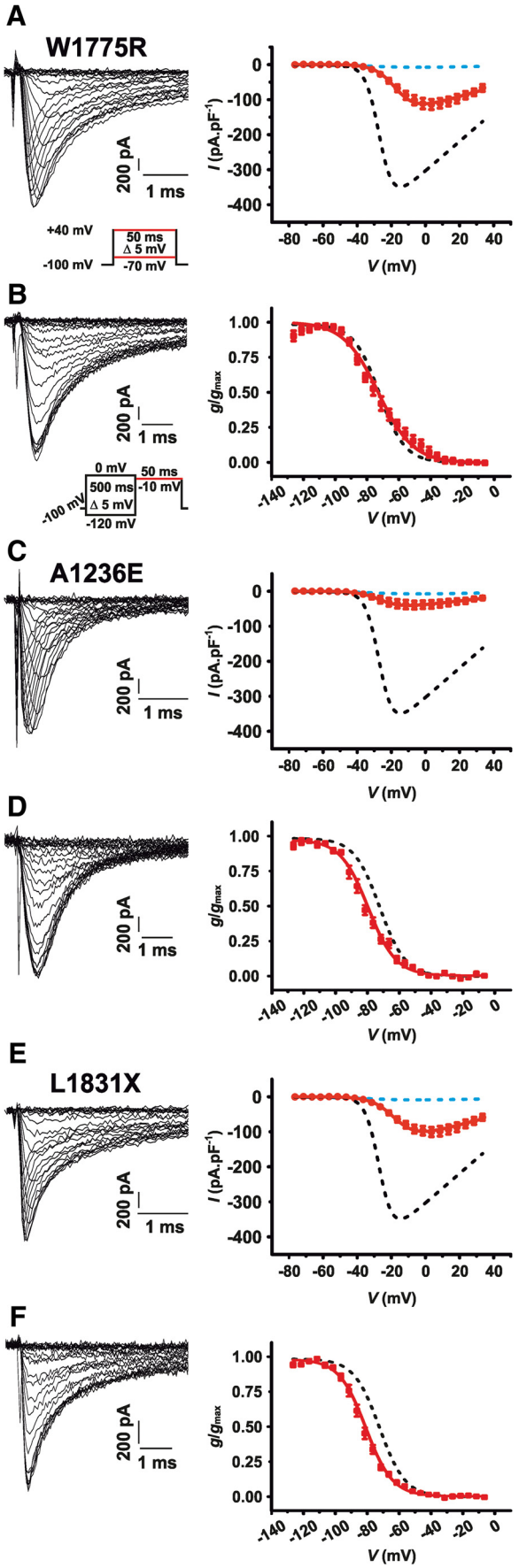

Figure 2. Electrophysiological characterization of W1775R, A1236E, and L1831X in HEK293 cells. For each trace, averaged WT (black dash) and β_1/β_2 only (blue dash) traces are overlaid.

mately contribute toward a loss of $Na_V1.7$ function. Nonetheless, our findings suggest that substantial, yet incomplete, block of $Na_V1.7$ and modulation of channel activation/inactivation properties might be sufficient for pain therapy. Interestingly, a patient has previously been reported with "partial congenital insensitivity to pain" who is a compound heterozygote for a 1 bp splice donor deletion midway through the *SCN9A* gene and a C1719R missense mutation (which maps upstream of the C-terminal intracellular region) (Staud et al., 2011). Although no biophysical analysis was performed, it was speculated by the authors that the incomplete pain insensitivity seen in the patient may be consistent with hypomorphic effects of one or both mutations. In contrast, the two families we describe appear to have complete pain insensitivity (although one patient lacked any injuries to her lips, tongue, or terminal digits often seen in other individuals with congenitally inherited insensitivity to pain) but carried mutations with at least some residual activity.

The C-terminal region of the voltage-gated sodium channel family is well conserved, with an EF-hand and downstream IQ motif annotated and verified in several Na_V channels (Wingo et al., 2004; Kubota et al., 2009; Miloushev et al., 2009). The $Na_V1.7$-W1775 residue, which is mutated in CIP Family 2, is completely conserved across all human Na_V family members, and the analogous amino acid in the cardiac sodium channel, $Na_V1.5$ (W1798) is known to be located within the first of 2 EF-hands. EF-hands are helix-loop-helix structural domains found in a large family of calcium binding proteins. The EF-hand of voltage-gated sodium channels is known to bind and stabilize the fast inactivation gate and also binds with beta1 and beta3 subunits (Spampanato et al., 2004; Cusdin et al., 2010). Mutations within C-terminal EF-hands of human Na_V channels have previously been reported to cause diseases, such as potassium-aggravated myonia and Long QT syndrome (Kubota et al., 2009; Glaaser et al., 2012). Downstream of the EF-hand is a calmodulin-binding IQ motif, which can modulate Na_V currents (Mori et al., 2003;

←

Comparisons to WT values are shown in Table 1. ***A***, Left, Representative raw trace of W1775R channel currents in response to the channel pulse protocol shown (activation). Right, Current–voltage relationship of the peak activation currents normalized to cell size (pA/pF) for W1775R (red). All traces were fitted with a Boltzmann equation (see Materials and Methods), where $V_{0.5} = -13.4 \pm 1.3$ mV, $k = -7.5 \pm 0.2$, $V_{Rev} = 71.4 \pm 4.9$ mV, and $I_{Max} = -115.9 \pm 15.0$ pA/pF ($n = 7$). ***B***, Left, Representative raw trace of W1775R currents in response to a test pulse to −10 mV following a series of prepulses (protocol shown in inset; fast inactivation). Right, Peak fast inactivation currents for W1775R (red) were normalized to the maximum current and plotted against the prepulse potential used. Data were fitted with a Boltzmann equation (see Materials and Methods), where $V_{0.5} = -73.4 \pm 2.2$ mV and $k = 11.6 \pm 1.1$ ($n = 7$). ***C***, Left, Representative raw trace of A1236E channel currents in response to the channel pulse protocol. Right, Current–voltage relationship of the peak activation currents normalized to cell size (pA/pF) for A1236E (red). All traces were fitted with a Boltzmann equation, where $V_{0.5} = -21.5 \pm 1.8$ mV, $k = -7.3 \pm 0.4$, $V_{Rev} = 67.5 \pm 3.8$ mV, and $I_{Max} = -41.0 \pm 11.9$ pA/pF ($n = 8$). ***D***, Left, Representative raw trace of A1236E currents in response to a test pulse to −10 mV following a series of prepulses as in ***B***. Right, Peak fast inactivation currents for A1236E (red) were normalized to the maximum current and plotted against the prepulse potential used. Data were fitted with a Boltzmann, where $V_{0.5} = -80.7 \pm 1.3$ mV and $k = 9.1 \pm 0.8$ ($n = 8$). ***E***, Left, Representative raw trace of L1831X channel currents in response to the channel pulse protocol. Right, Current–voltage relationship of the peak activation currents normalized to cell size (pA/pF) for L1831X (red). All traces were fitted with a Boltzmann equation, where $V_{0.5} = -15.4 \pm 1.8$ mV, $k = -7.6 \pm 0.2$, $V_{Rev} = 72.5 \pm 5.3$ mV, and $I_{Max} = -103.3 \pm 14.0$ pA/pF ($n = 9$). ***F***, Left, Representative raw trace of L1831X currents in response to a test pulse to −10 mV following a series of prepulses. Right, Peak fast inactivation currents for L1831X (red) were normalized to the maximum current and plotted against the prepulse potential used. Data were fitted with a Boltzmann equation, where $V_{0.5} = -82.2 \pm 1.3$ mV and $k = 7.9 \pm 0.6$ ($n = 9$).

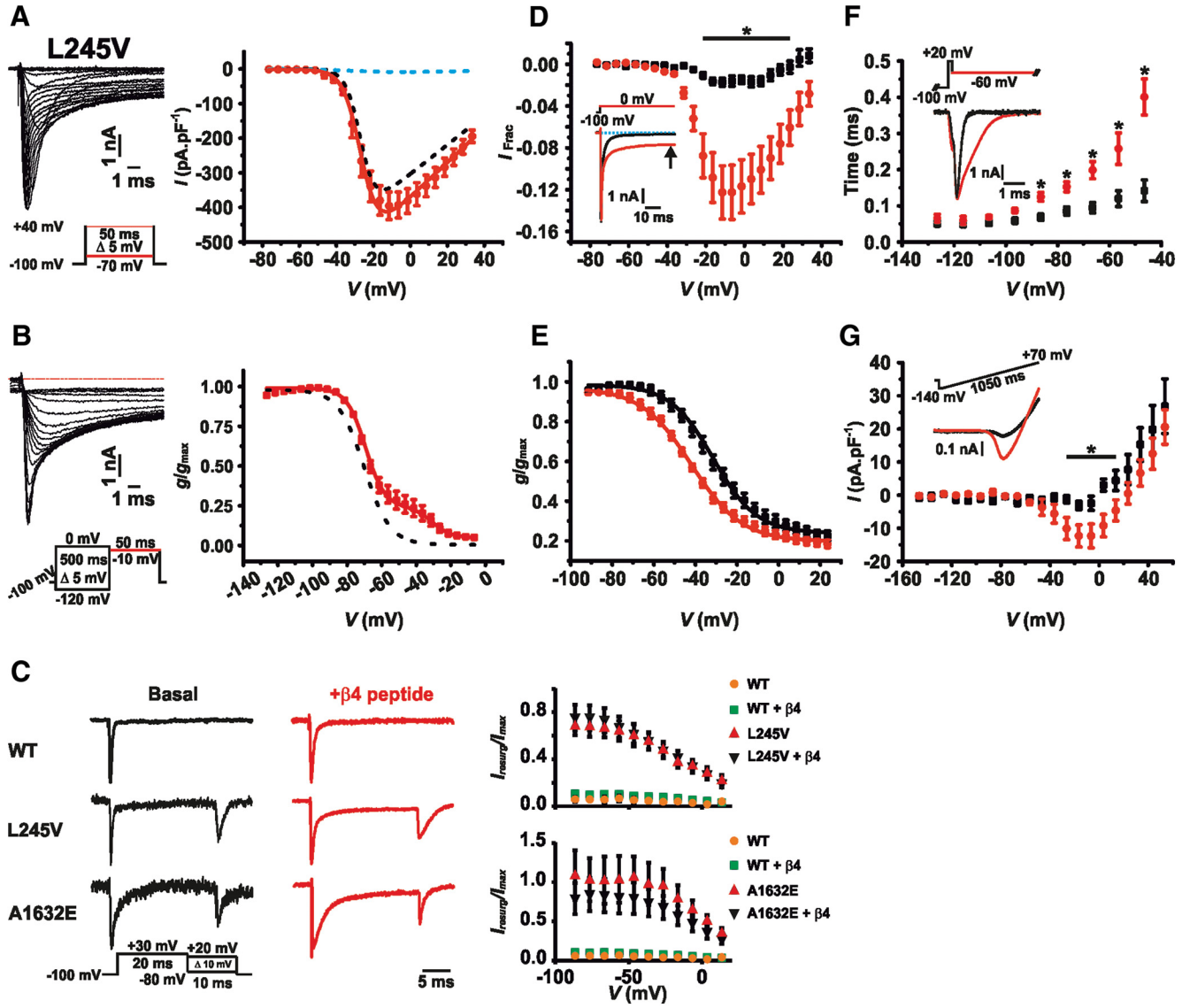

Figure 3. Electrophysiological characterization of L245V in HEK293 cells. ***A***, Left, Representative raw trace of L245V channel currents in response to the pulse protocol shown (activation). Right, Current–voltage relationship of the peak activation currents normalized to cell size (pA/pF) for L245V (red). Averaged WT (black dash) and β_1/β_2 only (blue dash) traces are overlaid. All traces were fitted with a Boltzmann equation (see Materials and Methods), where $V_{0.5} = -25.2 \pm 1.3$ mV, $k = -4.9 \pm 0.4$, $V_{Rev} = 74.0 \pm 3.1$ mV, and $I_{Max} = -398 \pm 44.7$ pA/pF ($n = 16$). Comparisons to WT values are shown in Table 1. ***B***, Left, Representative raw trace of L245V currents in response to a test pulse to −10 mV following a series of prepulses (protocol shown; fast inactivation). Right, Peak fast inactivation currents for L245V (red) were normalized to the maximum current and plotted against the prepulse potential used. Averaged WT (black dash) traces are overlaid. L245V traces were fitted with a double Boltzmann equation (see Materials and Methods), where $V_{0.5\#1} = -71.2 \pm 0.6$ mV and $V_{0.5\#2} = -31.4 \pm 1.8$ mV ($n = 14$). Comparisons to WT values are shown in Table 1. ***C***, Left, Representative tail current traces measured at −40 mV from wt, L245V, and A1632E expressing cells without (black) and with (red) addition of β4-peptide in the intracellular pipette solution. The voltage-stimulus protocol is shown below. Right, Compared with WT, the mutations L245V (top) and A1632E (bottom) cause a significant increase ($p < 0.05$) in tail current, measured as a fraction of the peak activation current at voltages between −80 and −20 mV; there was no significant difference between L245V and A1632E or between the presence and absence of the β4-peptide (two-way repeated-measures ANOVA with Bonferroni *post hoc*; $n = 3$–7). ***D***, Remaining current fraction (fraction of maximal peak current) at 50 ms following a series of depolarizing voltage steps from −100 mV to 40 mV. Inset, Averaged raw traces for WT (black) and L245V (red) in response to a single voltage step. *$p < 0.05$, individual comparisons. $p = 0.0026$, WT versus L245V group comparison (two-way repeated-measures ANOVA with Bonferroni *post hoc*; $n = 12$–16). ***E***, Peak slow-inactivation currents were obtained for L245V (red) and WT (black) by applying an extended conditioning pulse (10 s) ranging from −100 mV to 30 mV before stepping to −120 mV for 100 ms to recover channels from the fast inactivated state followed by a test pulse at −10 mV for 20 ms. Analysis shows peak currents, normalized to maximal current, obtained at the final −10 mV test pulse plotted against the prepulse potential. Data are fitted with a Boltzmann equation (see Materials and Methods) where: for the WT channels, $V_{0.5} = -31.43 \pm 1.8$ mV and $k = 9.9 \pm 0.6$; and for the L245V channels, $V_{0.5} = -41.36 \pm 0.9$ mV and $k = 11.3 \pm 1.7$ ($n = 8$–16). Comparisons are shown in Table 1. ***F***, Rate of channel deactivation following a brief depolarizing step to 20 mV (0.4 ms) from a holding potential of −100 mV before going to a final potential ranging from −120 mV to −40 mV. Inset, Averaged raw traces for WT (black) and L245V (red) when a final voltage step to −60 mV is applied. *$p < 0.05$, individual comparisons. $p < 0.0001$, WT versus L245V group comparison (two-way repeated-measures ANOVA with Bonferroni *post hoc*; $n = 10$–14). ***G***, Analysis of inward currents during a depolarizing ramp stimulus from −140 mV to 70 mV. Inset, Average raw traces for WT (black) and L245V (red) in response to the test pulse applied. *$p < 0.05$, individual comparisons. $p = 0.0266$, WT versus L245V group comparison (two-way repeated-measures ANOVA with Bonferroni *post hoc*; $n = 12$–15).

Reddy Chichili et al., 2013). In CIP Family 3, there is a truncating mutation (L1831X) that causes deletion of this IQ motif from the C terminus of the mutant $Na_V1.7$ channel. The mutations reported here highlight the importance of this region of the channel for normal function.

In contrast to loss-of-function mutations, we also characterized the novel IEM-associated mutation, L245V. Until recently, mutations in $Na_V1.7$ that give rise to the hypersensitive pain conditions IEM or PEPD have been functionally distinguished by exhibiting either a hyperpolarizing shift in channel activation or a

depolarizing shift in channel inactivation, respectively (Dib-Hajj et al., 2013). Here, however, we showed that, unlike typical IEM-associated mutations, L245V exhibited no shift in the voltage dependence of channel activation. This is consistent with other recently identified IEM-associated mutations. Eberhardt et al. (2014) recently presented an IEM mutation (A1632T) that had no change in channel activation but instead displayed a depolarizing shift in the voltage dependence of fast inactivation. The apparent lack of a shift in channel activation was also evident following the characterization of another IEM-associated mutation, G616R (Choi et al., 2010). These findings therefore question the validity of using a single marker to determine whether a mutation is IEM or PEPD causing.

Despite there being no change in channel activation, L245V did have changes in other gating characteristics, exhibiting incomplete fast inactivation, a hyperpolarizing shift in slow inactivation, a slowing of channel deactivation, the emergence of persistent and associated tail currents, as well as increased ramp currents. Understanding the relevance these changes have in predetermining an IEM or PEPD phenotype is difficult, as there is a significant overlap between changes in $Na_V1.7$ function and pathogenesis; a slowing of channel deactivation, the presence of persistent currents, as well as an increase in ramp current density have all been previously associated with both IEM and PEPD phenotypes (Lampert et al., 2006; Cheng et al., 2008, 2011; Choi et al., 2011; Eberhardt et al., 2014). More recently, it has been suggested that, in the absence of a shift in channel activation, the presence of persistent and resurgent currents is likely a determinant of whether a mutation is IEM or PEPD causing (Jarecki et al., 2010; Theile et al., 2011; Eberhardt et al., 2014). This, however, is not supported by the significant persistent and associated tail current presented here by L245V. Other electrophysiological characteristic indicators that have been proposed to distinguish IEM from PEPD include the effects associated mutations have on neuronal physiology. It has been suggested that, although both IEM and PEPD mutations lower the action potential threshold and enhance action potential firing from sensory neurons when overexpressed in DRG cultures, IEM-associated, but not PEPD-associated, mutations typically cause a depolarization of the resting membrane potential (Dib-Hajj et al., 2010). Although not directly studied here for L245V, Eberhardt et al. (2014) showed that the IEM-associated A1632T mutation did enhance excitability but had no effect on the resting membrane potential of sensory nerves. They concluded that the presence of persistent and resurgent currents is a characteristic hallmark for PEPD-associated mutations; however, in contrast to this, we clearly observed persistent currents for the IEM-associated L245V mutation, and a recent publication showed that application of the sea-anemone toxin ATX-II elicited resurgent currents predominantly in A-δ fibers, associated with a pricking/tingling pain rather than the burning pains reported in IEM and PEPD, which are thought to be mostly C-fiber mediated (Klinger et al., 2012).

Phenotype prediction arising from mutations in SCN9A

Understanding the etiology of *SCN9A*-associated hyposensitive and hypersensitive pain conditions is central to the development of therapies aimed at treating these debilitating disorders. Within recent years, much has been done to try and further understand the role $Na_V1.7$ channels have in the regulation of neuronal excitability and pain; however, the current mismatch between functional change and clinical phenotype suggests that phenotype-prediction arising from mutations in *SCN9A* is complex and unlikely to be determined by any single change in channel function. As presented here, both hyposensitive and hypersensitive pain conditions arising from mutations in *SCN9A* are likely to be determined by the overall functionality of $Na_V1.7$ channels as described by all gating parameters in addition to the size of the current passed.

References

Ahmad S, Dahllund L, Eriksson AB, Hellgren D, Karlsson U, Lund PE, Meijer IA, Meury L, Mills T, Moody A, Morinville A, Morten J, O'Donnell D, Raynoschek C, Salter H, Rouleau GA, Krupp JJ (2007) A stop codon mutation in SCN9A causes lack of pain sensation. Hum Mol Genet 16: 2114–2121. CrossRef Medline

Cheng X, Dib-Hajj SD, Tyrrell L, Waxman SG (2008) Mutation I136V alters electrophysiological properties of the Na(v)1.7 channel in a family with onset of erythromelalgia in the second decade. Mol Pain 4:1. CrossRef Medline

Cheng X, Dib-Hajj SD, Tyrrell L, Te Morsche RH, Drenth JP, Waxman SG (2011) Deletion mutation of sodium channel Na(V)1.7 in inherited erythromelalgia: enhanced slow inactivation modulates dorsal root ganglion neuron hyperexcitability. Brain 134:1972–1986. CrossRef Medline

Choi JS, Cheng X, Foster E, Leffler A, Tyrrell L, Te Morsche RH, Eastman EM, Jansen HJ, Huehne K, Nau C, Dib-Hajj SD, Drenth JP, Waxman SG (2010) Alternative splicing may contribute to time-dependent manifestation of inherited erythromelalgia. Brain 133:1823–1835. CrossRef Medline

Choi JS, Boralevi F, Brissaud O, Sánchez-Martin J, Te Morsche RH, Dib-Hajj SD, Drenth JP, Waxman SG (2011) Paroxysmal extreme pain disorder: a molecular lesion of peripheral neurons. Nat Rev Neurol 7:51–55. CrossRef Medline

Cox JJ, Reimann F, Nicholas AK, Thornton G, Roberts E, Springell K, Karbani G, Jafri H, Mannan J, Raashid Y, Al-Gazali L, Hamamy H, Valente EM, Gorman S, Williams R, McHale DP, Wood JN, Gribble FM, Woods CG (2006) An SCN9A channelopathy causes congenital inability to experience pain. Nature 444:894–898. CrossRef Medline

Cox JJ, Sheynin J, Shorer Z, Reimann F, Nicholas AK, Zubovic L, Baralle M, Wraige E, Manor E, Levy J, Woods CG, Parvari R (2010) Congenital insensitivity to pain: novel SCN9A missense and in-frame deletion mutations. Hum Mutat 31:E1670–E1686. CrossRef Medline

Cusdin FS, Nietlispach D, Maman J, Dale TJ, Powell AJ, Clare JJ, Jackson AP (2010) The sodium channel β3-subunit induces multiphasic gating in NaV1.3 and affects fast inactivation via distinct intracellular regions. J Biol Chem 285:33404–33412. CrossRef Medline

Dib-Hajj SD, Estacion M, Jarecki BW, Tyrrell L, Fischer TZ, Lawden M, Cummins TR, Waxman SG (2008) Paroxysmal extreme pain disorder M1627K mutation in human Nav1.7 renders DRG neurons hyperexcitable. Mol Pain 4:37. CrossRef Medline

Dib-Hajj SD, Cummins TR, Black JA, Waxman SG (2010) Sodium channels in normal and pathological pain. Annu Rev Neurosci 33:325–347. CrossRef Medline

Dib-Hajj SD, Yang Y, Black JA, Waxman SG (2013) The Na(V)1.7 sodium channel: from molecule to man. Nat Rev Neurosci 14:49–62. CrossRef Medline

Eberhardt M, Nakajima J, Klinger AB, Neacsu C, Hühne K, O'Reilly AO, Kist AM, Lampe AK, Fischer K, Gibson J, Nau C, Winterpacht A, Lampert A (2014) Inherited pain: sodium channel Nav1.7 A1632T mutation causes erythromelalgia due to a shift of fast inactivation. J Biol Chem 289:1971–1980. CrossRef Medline

Estacion M, Dib-Hajj SD, Benke PJ, Te Morsche RH, Eastman EM, Macala LJ, Drenth JP, Waxman SG (2008) NaV1.7 gain-of-function mutations as a continuum: A1632E displays physiological changes associated with erythromelalgia and paroxysmal extreme pain disorder mutations and produces symptoms of both disorders. J Neurosci 28:11079–11088. CrossRef Medline

Faber CG, Hoeijmakers JG, Ahn HS, Cheng X, Han C, Choi JS, Estacion M, Lauria G, Vanhoutte EK, Gerrits MM, Dib-Hajj S, Drenth JP, Waxman SG, Merkies IS (2012) Gain of function Nanu1.7 mutations in idiopathic small fiber neuropathy. Ann Neurol 71:26–39. CrossRef Medline

Gingras J, Smith S, Matson DJ, Johnson D, Nye K, Couture L, Feric E, Yin R, Moyer BD, Peterson ML, Rottman JB, Beiler RJ, Malmberg AB, McDonough SI (2014) Global Nav1.7 knockout mice recapitulate the phenotype of human congenital indifference to pain. PLoS One 9:e105895. CrossRef Medline

Glaaser IW, Osteen JD, Puckerin A, Sampson KJ, Jin X, Kass RS (2012) Perturbation of sodium channel structure by an inherited Long QT Syndrome mutation. Nat Commun 3:706. CrossRef Medline

Jarecki BW, Piekarz AD, Jackson JO 2nd, Cummins TR (2010) Human voltage-gated sodium channel mutations that cause inherited neuronal and muscle channelopathies increase resurgent sodium currents. J Clin Invest 120:369–378. CrossRef Medline

Klinger AB, Eberhardt M, Link AS, Namer B, Kutsche LK, Schuy ET, Sittl R, Hoffmann T, Alzheimer C, Huth T, Carr RW, Lampert A (2012) Sea-anemone toxin ATX-II elicits A-fiber-dependent pain and enhances resurgent and persistent sodium currents in large sensory neurons. Mol Pain 8:69. CrossRef Medline

Kubota T, Kinoshita M, Sasaki R, Aoike F, Takahashi MP, Sakoda S, Hirose K (2009) New mutation of the Na channel in the severe form of potassium-aggravated myotonia. Muscle Nerve 39:666–673. CrossRef Medline

Lampert A, Dib-Hajj SD, Tyrrell L, Waxman SG (2006) Size matters: erythromelalgia mutation S241T in Nav1.7 alters channel gating. J Biol Chem 281:36029–36035. CrossRef Medline

Miloushev VZ, Levine JA, Arbing MA, Hunt JF, Pitt GS, Palmer AG 3rd (2009) Solution structure of the NaV1.2 C-terminal EF-hand domain. J Biol Chem 284:6446–6454. CrossRef Medline

Mori M, Konno T, Morii T, Nagayama K, Imoto K (2003) Regulatory interaction of sodium channel IQ-motif with calmodulin C-terminal lobe. Biochem Biophys Res Commun 307:290–296. CrossRef Medline

Reddy Chichili VP, Xiao Y, Seetharaman J, Cummins TR, Sivaraman J (2013) Structural basis for the modulation of the neuronal voltage-gated sodium channel NaV1.6 by calmodulin. Sci Rep 3:2435. CrossRef Medline

Spampanato J, Kearney JA, de Haan G, McEwen DP, Escayg A, Aradi I, MacDonald BT, Levin SI, Soltesz I, Benna P, Montalenti E, Isom LL, Goldin AL, Meisler MH (2004) A novel epilepsy mutation in the sodium channel SCN1A identifies a cytoplasmic domain for beta subunit interaction. J Neurosci 24:10022–10034. CrossRef Medline

Staud R, Price DD, Janicke D, Andrade E, Hadjipanayis AG, Eaton WT, Kaplan L, Wallace MR (2011) Two novel mutations of SCN9A (Nav1.7) are associated with partial congenital insensitivity to pain. Eur J Pain 15:223–230. CrossRef Medline

Theile JW, Jarecki BW, Piekarz AD, Cummins TR (2011) Nav1.7 mutations associated with paroxysmal extreme pain disorder, but not erythromelalgia, enhance Navbeta4 peptide-mediated resurgent sodium currents. J Physiol 589:597–608. CrossRef Medline

Wingo TL, Shah VN, Anderson ME, Lybrand TP, Chazin WJ, Balser JR (2004) An EF-hand in the sodium channel couples intracellular calcium to cardiac excitability. Nat Struct Mol Biol 11:219–225. CrossRef Medline